NANO LETTERS

Letter

pubs.acs.org/NanoLett

Mechanical Properties of Silicon Carbide Nanowires: Effect of Size-Dependent Defect Density

Guangming Cheng,[†] Tzu-Hsuan Chang,[†] Qingquan Qin,[†] Hanchen Huang,[‡] and Yong Zhu*[,†]

[†]Department of Mechanical and Aerospace Engineering, North Carolina State University, Raleigh, North Carolina 27695, United States

[‡]Department of Mechanical and Industrial Engineering, Northeastern University, Boston, Massachusetts 02115, United States

Supporting Information

ABSTRACT: This paper reports quantitative mechanical characterization of silicon carbide (SiC) nanowires (NWs) via in situ tensile tests inside scanning electron microscopy using a microelectromechanical system. The NWs are synthesized using the vapor−liquid−solid process with growth direction of ⟨111⟩. They consist of three types of structures, pure face-centered cubic (3C) structure, 3C structure with an inclined stacking fault (SF), and highly defective structure, in a periodic fashion along the NW length. The SiC NWs are found to deform linear elastically until brittle fracture. Their fracture origin is identified in the 3C structures with inclined SFs, rather than the highly defective structures. The fracture strength increases as the NW diameter decreases from 45 to 17 nm, approaching the theoretical strength of 3C SiC. The size effect on fracture strength of SiC NWs is attributed to the size-dependent defect density rather than the surface effect that is dominant for single crystalline NWs.

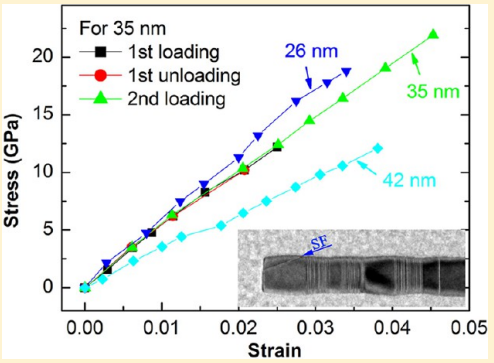

KEYWORDS: *Size effect, ultrahigh strength, in situ tensile testing, brittle fracture, nanomechanics*

Silicon carbide (SiC) has high mechanical strength, high thermal conductivity, and variable band gaps, in addition to other superior properties such as radiation resistance.[1−3] These properties make SiC a suitable material operating at high temperature, high power, and high frequency as well as in harsh environments. SiC nanowires (NWs) have been used in a number of mechanical and electronic applications.[4,5] For instance, a small addition of SiC NWs into a SiC whisker-reinforced matrix was found to double the toughness of the nanocomposite.[6] SiC nanoresonators are capable of yielding substantially higher frequencies than GaAs and Si counterparts for given dimensions.[7] The operation and reliability of these nanoscale structures and devices depend on the mechanical properties of SiC NWs, which are expected to be different from their bulk counterparts due to increasing surface-to-volume ratio.

However, investigations on the mechanical properties of SiC NWs have been scarce. Han et al. performed qualitative in situ transmission electron microscopy (TEM) tension tests of SiC NWs and found substantial plasticity at room temperature (e.g., ⟨111⟩ SiC NWs experience over 200% elongation before fracture).[8] This observation is somewhat surprising in view that SiC whiskers are brittle at room temperature and is possibly due to electron-irradiation-induced phase transformation from crystalline to amorphous structure. Among the atomistic simulations, discrepancies also exist on the brittle or ductile nature of SiC NWs. Molecular dynamics (MD) simulations showed that SiC NWs deform elastically under tensile loading followed by brittle failure.[9] Wang et al. simulated the mechanical properties of SiC NWs with several different microstructures.[10] They found that almost all the microstructures lead to brittle failure with one exception. In that case, plastic deformation was predicted in 3C structure with an intergranular amorphous film parallel to the {111} plane and inclined at an angle of 19.47° with respect to the NW axis.

Lieber and co-workers reported the first measurement of the fracture strength of SiC NWs using atomic force microscopy based bending tests.[11] They reported that the maximum fracture strength of SiC NWs was 53.4 GPa, which is much larger than the corresponding values for bulk SiC and microscale SiC whiskers. However, the fracture strength of SiC NWs was not studied systematically as a function of the NW size. In addition, SiC NWs have quite complicated microstructures due to the coexistence of polytypes.[12] SiC could be face-centered cubic (i.e., 3C or β-SiC), hexagonal-close-packed (i.e., 2H-SiC), or other highly ordered structures (e.g., 4H and 6H). Stacking faults (SFs) are also common in SiC due to the low SF energy. Therefore, it is of important relevance to identify which polytype or microstructure is more prone to fracture.

Here we report, for the first time, quantitative stress−strain measurements of SiC NWs via in situ tensile testing inside

Received: October 31, 2013
Revised: December 12, 2013

   dx.doi.org/10.1021/nl404058r | *Nano Lett.* XXXX, XXX, XXX−XXX

scanning electron microscopy (SEM). The NWs tested were synthesized using the vapor−liquid−solid (VLS) process with growth direction of ⟨111⟩. The SiC NWs consist of three types of structures, pure 3C structure, 3C structure with an inclined SF, and highly defective structure, in a periodic fashion along the NW length. Our tensile tests showed that the SiC NWs deformed linear elastically until brittle fracture. The fracture origin in SiC NWs was identified in the 3C segments with inclined SFs. The fracture strength increased as the NW diameter decreased up to over 25 GPa, approaching the theoretical strength of 3C SiC.

The SiC NWs were synthesized by using high-temperature thermal evaporation through the vapor−liquid−solid process.[13] The source materials are SiO2 and C powder with Fe powder as catalyst. The mixture of these materials evaporates at 1500 °C, moves downstream with argon flow and deposits on an Al_2O_3 substrate at about 800 °C. All NW samples for mechanical testing and TEM observation were etched in a mixture of HF (48%) and ethanol with a ratio of 1:4 to remove the oxide layer on the NW surfaces. Figure 1a shows a low-magnification TEM image of the SiC NWs. The NW growth direction is ⟨111⟩. Most NWs are straight, while some are kinky. The straight NWs are globally uniform in diameter along the growth direction except local undulations. Figure 1b shows a histogram of the NW diameter based on 500 NWs. It can be seen that the SiC NWs range from a few nanometer to ~60 nm in diameter with the average diameter of ~25 nm. Figure 1c shows a Raman spectrum of the SiC NWs. The spectrum exhibits two stronger and broadening peaks at 789 and 955 cm^{-1}. The peak centered at 789 cm^{-1} was attributed to a transverse optical (TO) modes and the one at 955 cm^{-1} to the longitudinal optical (LO) modes.[14] With respect to the bulk 3C-SiC (796 and 972 cm^{-1}), the Raman frequency is shifted about 7−17 cm^{-1}, which is attributed to the presence of polytypic admixtures (e.g., nanotwins or SFs are equivalent to a polytypic admixture in SiC).[5]

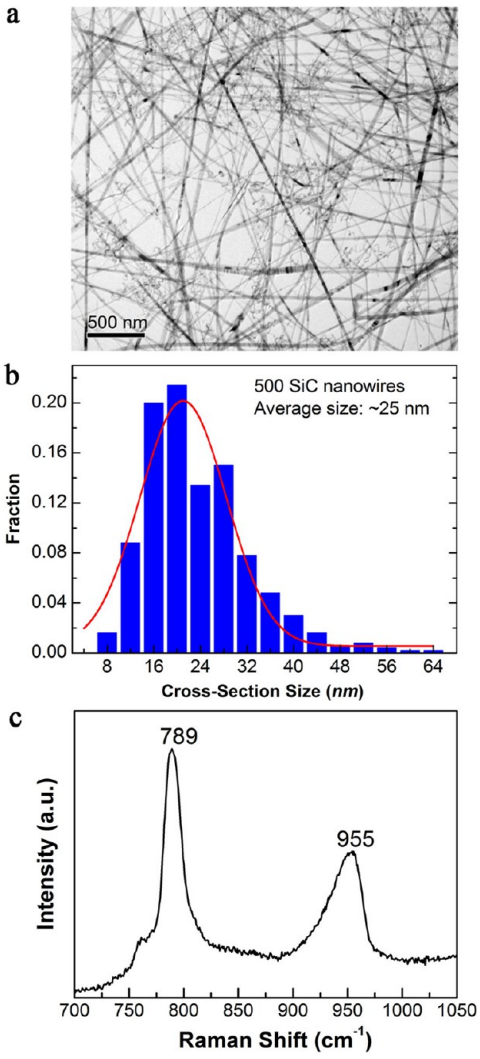

Figure 1. (a) Low-magnified TEM image of a large number of randomly oriented SiC NWs. (b) Histogram of the NW diameter distribution (8−64 nm). (c) Raman spectrum of SiC NWs.

TEM imaging of individual SiC NWs indicates that the NW consists of pure 3C structures, 3C structures with inclined SFs (i.e., 19.47° with respect to the NW axis), and highly defective structures in a periodic fashion. Figure 2a shows a low-magnification TEM image of the NW with the growth direction of ⟨111⟩, where the 3C structure with a 19.47° SF, highly defective structure and pure 3C structure are marked by I, II, and III, respectively, and are separated by dashed lines. TEM images of more NWs with the three types of structures are provided in the Supporting Information. Figure 2b is a high-resolution TEM (HRTEM) image corresponding to the boxed area in Figure 2a. The two segments indicated by A and B in Figure 2b are 3C structure with a 19.47° SF (labeled as SF-19.47°) and highly defective structure, respectively. The insets in Figures 2b are the corresponding fast Fourier transformed (FFT) diffraction patterns taken from the areas A and B along zone axis of ⟨110⟩. Figure 2c is a magnified HRTEM image corresponding to the boxed area in segment B (Figure 2b), which contains several types of distinctive atomic structures including nanotwins, intrinsic SFI, and extrinsic SFII. Such defective structures might contribute to the Raman shift in Figure 1c. An interesting question would be which segment fails first upon tensile loading on the NW. Details of the fracture surfaces will be further studied by post-mortem TEM observations later.

In situ SEM tensile tests of SiC NWs were performed using a microelectromechanical system (MEMS).[15−17] The MEMS stage consists of a thermal actuator and a differential capacitive load sensor with a gap in between (Figure 3a). The inset shows an individual SiC NW that is mounted across the gap. The MEMS stage was fabricated at MEMSCAP (Durham, NC) using the silicon-on-insulator multi-user MEMS processes (SOI-MUMPs). During each test, load is applied using the thermal actuator on one side of the specimen and is measured using the differential capacitive load sensor on the other side.[18] An individual NW was picked from the as-grown substrate using a nanomanipulator (Klocke Nanotechnik, Germany) inside SEM and mounted onto the MEMS stage.[15] The NW was clamped on the MEMS stage by electron beam induced deposition of carbonaceous materials in the SEM chamber. During each test, a sequence of SEM images was taken. The NW strain was then calculated by digital image correlation of the SEM images, giving a resolution of 0.03%.[19−21] With a force resolution of 12 nN,[15] the stress resolution ranged from 52.9 to 7.5 MPa for the NW diameter ranging from 17 to 45 nm.

To study the size effects on the fracture strength of SiC NWs, a total of 18 NWs with diameters ranging from 17 to 45 nm were tested. All the NWs exhibited more or less linear elastic behavior until apparent brittle fracture occurred. Figure 3b

dx.doi.org/10.1021/nl404058r | Nano Lett. XXXX, XXX, XXX−XXX

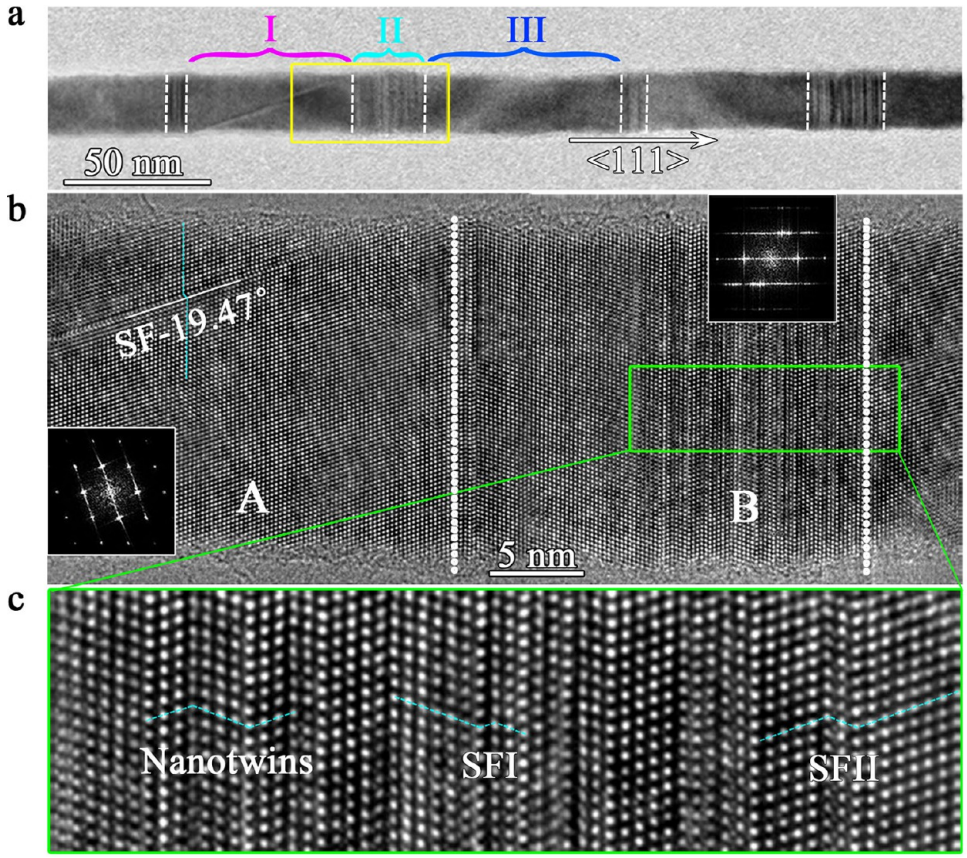

Figure 2. (a) A low-magnification TEM image of an individual SiC NW with the growth direction of ⟨111⟩, the 3C structure with an inclined SF, highly defective structure and pure 3C structure are marked by I, II, and III, respectively, and are separated by dashed lines. (b) HRTEM observation of the NW containing 3C structure with a 19.47° SF (segment A) and high-defective structures (segment B), corresponding to the boxed area in panel (a). Insets are the FFT diffraction patterns taken from areas A and B. Note that a 19.47° SF is present in the 3C segment, marked as SF-19.47°. (c) A magnified HRTEM image of the highly defective structure corresponding to the boxed area in (b) showing nanotwins, intrinsic SFI, and extrinsic SFII in the NW.

shows three representative stress−strain curves of the SiC NWs. The inset shows the fracture surface of a SiC NW that is typical of brittle fracture. In particular, multiple loading and unloading were conducted on some of the NWs (e.g., the one with diameter of 35 nm), which confirmed that the SiC NWs are linear elastic until brittle fracture.

Figure 3c shows the measured fracture strength as a function of the NW diameter. The fracture strength was strongly size dependent, increasing from 8.1 to 25.3 GPa as the diameter decreased from 45 to 17 nm. The highest fracture strength in our experiments is very close to the theoretical fracture strength of 3C SiC, 28.5 GPa, in the ⟨111⟩ direction.[10] Figure 3c also includes the fracture strength data of the SiC whiskers.[11,22−25] The collective data of whiskers and NWs show clear strengthening trend with decreasing diameter. The "smaller is stronger" trend has been observed in a number of single crystalline semiconductor and metallic NWs, where the surface effect plays the dominant role and the size effect can be interpreted by Weibull-type weakest link framework.[19,20,26−28] Note that while the weakest link explanation is typically employed for brittle materials, it has been applied to metallic NWs in view of the dislocation nucleation from free surfaces and nearly absence of preexisting dislocations in the NWs.[20,26]

However, no clear size effect on the Young's modulus was observed. The measured Young's moduli exhibited a large scatter (from 166 to 1270 GPa) with the average value of 531 GPa. The average value is within the range for bulk SiC (503−600 GPa) and the range of scatter is consistent with that of SiC whiskers (from 276 to 1516 GPa).[22] The large scatter for both SiC NWs and whiskers is likely due to the coexistence of polytypes and various types of defects.

Figure 3d shows the defect density as a function of the NW diameter. There are two types of defects (3C structure with a 19.47° SF and highly defective structure). As the diameter becomes smaller, the defect density of both types of defects reduces. Out of the three types of structures in SiC NWs, the pure 3C is the strongest, the highly defective structure is the second strongest, and the 3C structure with a 19.47° SF is the weakest, as predicted by MD simulations.[10] Our experimental results are consistent with the MD predictions. As shown in Figure 3d, when the NW diameter becomes smaller, the density of 3C structure with 19.47° SFs decreases, which leads to increase in fracture strength. Therefore, the size effect on fracture strength of SiC NWs is attributed to the size-dependent defect density (i.e., of the 3C structure with 19.47° SF), rather than the surface effect that is common to single crystalline NWs.

Postmortem TEM images showed that the fracture surfaces are perpendicular to the loading direction ⟨111⟩, which is typical of brittle fracture (Figure 4a). It is very interesting to note that the crack always initiated and propagated in a segment of 3C structure with a 19.47° SF, based on our post-

dx.doi.org/10.1021/nl404058r | Nano Lett. XXXX, XXX, XXX−XXX

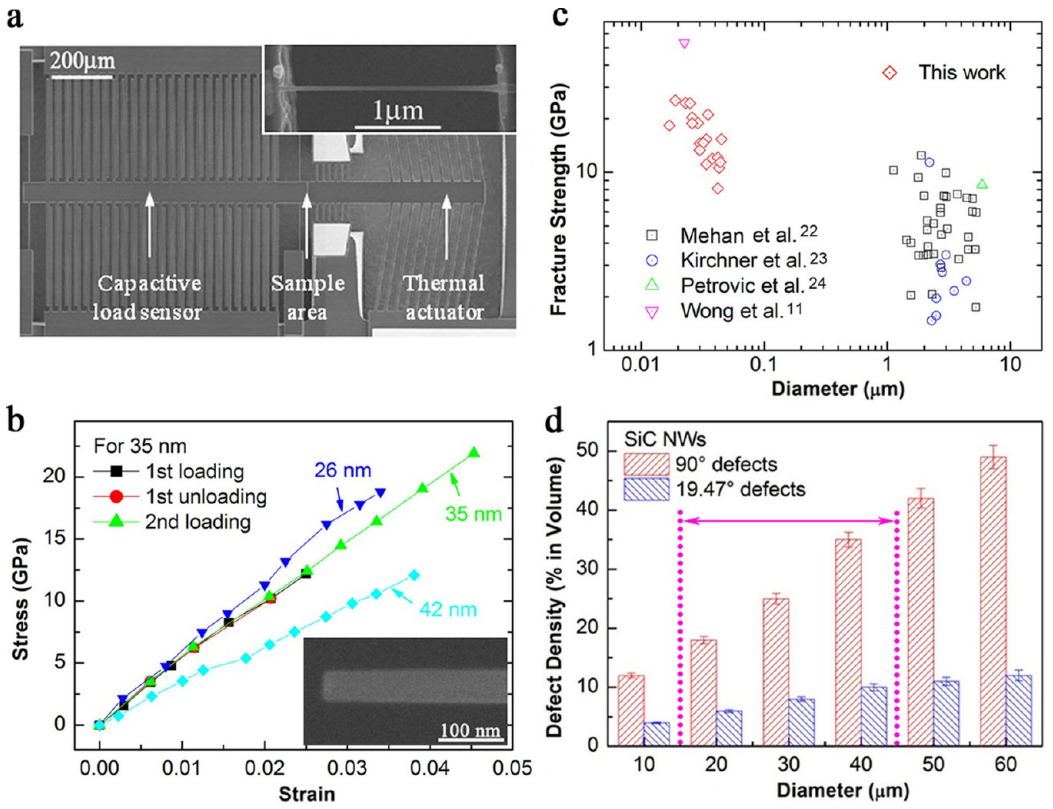

Figure 3. (a) The MEMS stage used for in situ SEM tensile testing of SiC NWs. Inset shows a NW bridged between the actuator and the load sensor. (b) Representative stress−strain curves of SiC NWs. The curve for the NW of 35 nm in diameter includes multiple loading and unloading, showing linear elastic behavior and brittle fracture. Inset shows the fracture surface of a SiC NW. (c) Fracture strength of SiC NWs and whiskers as a function of the diameter. (d) Defect density as a function of NW diameter. Note that the defect density is defined as an average volume percentage of defect parts in a randomly selected segment with a length of 2 μm. Here 90° and 19.47° defects refer to highly defective structures and 3C structures with a 19.47° SFs, respectively. The range between the dot lines corresponds to the diameter range tested in this work (17−45 nm).

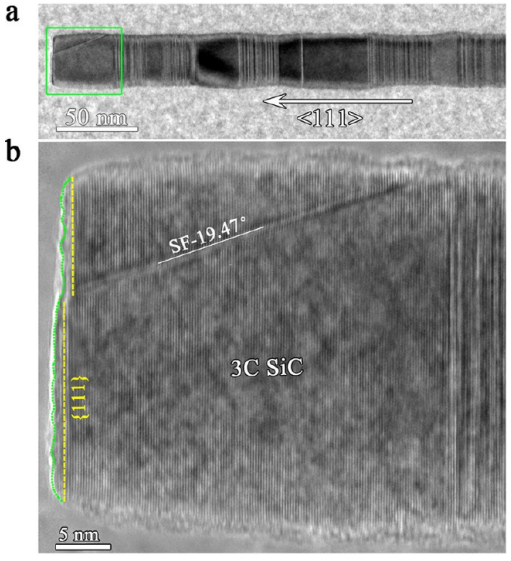

Figure 4. (a) Low-magnification TEM image of the fracture surface of a SiC NW. (b) HRTEM image of the fracture surface of the SiC NW, corresponding to the marked area in (a). The loading direction is along the ⟨111⟩ direction. The 19.47° SF is labeled as SF-19.47°. Similar fracture surfaces were observed other NWs tested (see the Supporting Information).

mortem HRTEM observations of 12 NWs (see additional examples in the Supporting Information). One reason is that the 3C segments are slightly tapered during synthesis and thus narrower than the twinned regions as synthesized (Figure 2a), leading to slightly higher stress in such segments. It should be emphasized that the slightly narrower fracture end in Figure 4b was as synthesized, not an indication of necking.

Another and more likely reason is that the 3C segments with 19.47° SFs are weaker than the segments with highly defective structures. Atomistic simulations predicted that the cracks initiate and propagate in the regions with periodic 90° nanotwins (twining plane perpendicular to the growth direction) or highly ordered structures (e.g., 4H, 6H, and so forth) in SiC NWs,[10,29,30] which is different from our observation. The highly defective structures in our SiC NWs are not pure nanotwins or highly ordered structures as in the simulations but composed of high density of randomly distributed nanotwins, SFs, and highly ordered structures. Each individual microstructure has a thickness of only several atomic layers, which is effective in blocking crack motion and leads to strengthening of the highly defective segments. Wang et al. systematically investigated the effect of different types of defects (especially, SFs and nanotwins) on the mechanical properties of SiC NWs by MD simulations.[10] They found that the NW strength decreases substantially with the increasing thickness of SFs that are 19.47° from the NW axial direction (e.g., decreasing by 29.5% from 28.5 GPa for pure 3C structure to 20.1 GPa with SF thickness of 5 nm). On the other hand, the NW strength decreases much less for 90° SFs or nanotwins (e.g., decreasing by 10.5% from 28.5 to 25.5 GPa with SF

dx.doi.org/10.1021/nl404058r | Nano Lett. XXXX, XXX, XXX−XXX

composition of 50%, and by 6.3% from 28.5 to 26.7 GPa with twin composition of 50%). It suggests that out of the three types of microstructures observed in our SiC NWs, the pure 3C structure is the strongest, the highly defective structure is the second strongest, and the 3C structure with 19.47° SF is the weakest. This result agrees well with our experimental observation that the cracks always initiate and propagate in the 3C segments with 19.47° SFs. The arrangement of a large number of 90° SFs and nanotwins in the highly defective structures are expected to play an important role in impeding crack propagation.

In conclusion, we have quantitatively studied the mechanical properties of SiC NWs. The microstructure of SiC NWs is rather complex, consisting of pure 3C structure, 3C structure with an inclined SF, and highly defective structure in a periodic fashion along the NW length. We found that the SiC NWs fail in brittle fracture at room temperature, in contrast to the superplasticity as previously observed. The SiC NWs exhibited strong size effect in the fracture strength; that is, the fracture strength increased with decreasing diameter up to over 25 GPa and approaching the theoretical strength of 3C SiC. It is interesting to observe that the cracks initiate and propagate in the 3C segments with the 19.47° SFs, rather than in the highly defective segments. The size effect on fracture strength of SiC NWs is attributed to the size-dependent defect density (i.e., of the 3C structure with 19.47° SFs), rather than the surface effect that is common to single crystalline NWs. Both bottom-up and top-down fabricated crystalline NWs often contain internal structures and defects (in addition to free surfaces). The present work indicates the importance to carefully examine the internal structures and defects in such NWs and understand their effects on the nanomechanical behaviors.

■ ASSOCIATED CONTENT

Supporting Information

Additional information and figures. This material is available free of charge via the Internet at http://pubs.acs.org.

■ AUTHOR INFORMATION

Corresponding Author

*E-mail: yong_zhu@ncsu.edu.

Notes

The authors declare no competing financial interest.

■ ACKNOWLEDGMENTS

This project was supported by the National Science Foundation under Award Nos. CMMI-1030637 and 1301193. The authors acknowledge the use of the Analytical Instrumentation Facility (AIF) at North Carolina State University, which is supported by the State of North Carolina and the National Science Foundation.

■ REFERENCES

(1) Persson, C. *Phys. Rev. B* **1996**, *54*, 10257−10260.
(2) Morkoc, H.; Strite, S.; Gao, G. B.; Lin, M. E.; Sverdlov, B.; Burns, M. *J. Appl. Phys.* **1994**, *76*, 1363.
(3) Huang, H. C.; Ghoniem, N. M. *J. Nucl. Mater.* **1993**, *199*, 221−230.
(4) Lu, W.; Lieber, C. M. *Nat. Mater.* **2007**, *6*, 841−850.
(5) Zekentes, K.; Rogdakis, K. *J. Phys. D. Appl. Phys.* **2011**, *44*, 133001.
(6) Yang, W.; Araki, H.; Tang, C.; Thaveethavorn, S.; Kohyama, A.; Suzuki, H.; Noda, T. *Adv. Mater.* **2005**, *17*, 1519−1523.
(7) Yang, Y. T.; Ekinci, K. L.; Huang, X. M. H.; Schiavone, L. M.; Roukes, M. L.; Zorman, C. A.; Mehregany, M. *Appl. Phys. Lett.* **2001**, *78*, 162.
(8) Zhang, Y. F.; Han, X. D.; Zheng, K.; Zhang, Z.; Zhang, X. N.; Fu, J. Y.; Ji, Y.; Hao, Y. J.; Guo, X. Y.; Wang, Z. L. *Adv. Funct. Mater.* **2007**, *17*, 3435−3440.
(9) Wang, Z. G.; Li, J. B.; Gao, F.; Weber, W. J. *Acta Mater.* **2010**, *58*, 1963−1971.
(10) Wang, J.; Lu, C.; Wang, Q.; Xiao, P.; Ke, F.; Bai, Y.; Shen, Y.; Liao, X.; Gao, H. *Nanotechnology* **2012**, *23*, 025703.
(11) Wong, E. W.; Sheehan, P. E.; Lieber, C. M. *Science* **1997**, *277*, 1971−1975.
(12) Wood, E. L.; Sansoz, F. *Nanoscale* **2012**, *4*, 5268−76.
(13) Shim, H. W.; Huang, H. C. *Appl. Phys. Lett.* **2007**, *90*, 083106.
(14) Gouadec, G.; Colomban, P. *Prog. Cryst. Growth Charact. Mater.* **2007**, *53*, 1−56.
(15) Zhu, Y.; Espinosa, H. D. *Proc. Natl. Acad. Sci. U.S.A.* **2005**, *102*, 14503−14508.
(16) Qin, Q.; Zhu, Y. *Appl. Phys. Lett.* **2013**, *102*, 013101.
(17) Zhu, Y.; Moldovan, N.; Espinosa, H. D. *Appl. Phys. Lett.* **2005**, *86*, 13506.
(18) Zhang, D.; Breguet, J.-M.; Clavel, R.; Sivakov, V.; Christiansen, S.; Michler, J. *J. Microelectromechanical Syst.* **2010**, *19*, 663−674.
(19) Zhu, Y.; Xu, F.; Qin, Q. Q.; Fung, W. Y.; Lu, W. *Nano Lett.* **2009**, *9*, 3934−3939.
(20) Zhu, Y.; Qin, Q. Q.; Xu, F.; Fan, F. R.; Ding, Y.; Zhang, T.; Wiley, B. J.; Wang, Z. L. *Phys. Rev. B* **2012**, *85*, 45443.
(21) Xu, F.; Qin, Q. Q.; Mishra, A.; Gu, Y.; Zhu, Y. *Nano Res* **2010**, *3*, 271−280.
(22) Mehan, R. L.; Herzog, J. A. In *Whisker Technology*; Levitt, A. P., Ed.; Wiley: New York, 1970; p 169.
(23) Kirchner, H.; Knoll, P. *J. Am. Ceram. Soc.* **1963**, *46*, 299−300.
(24) Petrovic, J. J.; Milewski, J. V; Rohr, D. L.; Gac, F. D. *J. Mater. Sci.* **1985**, *20*, 1167−1177.
(25) Bayer, P. D.; Cooper, R. E. *J. Mater. Sci.* **1967**, *2*, 233−237.
(26) Richter, G.; Hillerich, K.; Gianola, D. S.; Mönig, R.; Kraft, O.; Volkert, C. A. *Nano Lett.* **2009**, *9*, 3048−3052.
(27) Agrawal, R.; Peng, B.; Espinosa, H. D. *Nano Lett.* **2009**, *9*, 4177−4183.
(28) He, M. R.; Zhu, J. *Phys. Rev. B* **2011**, *83*, 161302.
(29) Li, Z.; Wang, S.; Wang, Z.; Zu, X.; Gao, F.; Weber, W. J. *J. Appl. Phys.* **2010**, *108*, 013504.
(30) Kim, T. Y.; Han, S. S.; Lee, H. M. *Mater. Trans.* **2004**, *45*, 1442−1449.

dx.doi.org/10.1021/nl404058r | *Nano Lett.* XXXX, XXX, XXX−XXX

Supporting Information

Mechanical Properties of Silicon Carbide Nanowires

Guangming Cheng[1], Tzu-Hsuan Chang[1], Qingquan Qin[1], Hanchen Huang[2] and Yong Zhu[1*]

[1]Department of Mechanical and Aerospace Engineering, North Carolina State University, Raleigh, NC 27695

[2]Department of Mechanical and Industrial Engineering, Northeastern University, Boston, MA 02115

* E-mail: yong_zhu@ncsu.edu

Figure S1 Bright-field TEM images of SiC NWs with a diameter of 18 and 41 nm in (a) and (b), respectively. Three types of structures, pure 3C structure, 3C structure with a 19.47^o SF and highly defective structure, can be seen. 19.47˚ stacking faults are marked by the blue arrows.

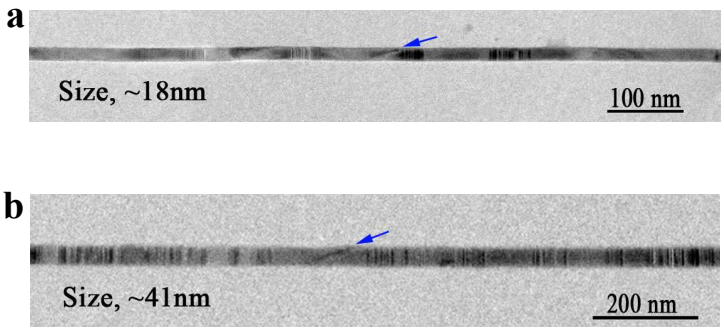

Figure S2 Bright-field TEM images show the fracture surfaces of SiC NWs. The fractures were always in the 3C segments with 19.47˚ stacking faults (marked by the blue arrows). **a** corresponds to the fracture surface in the text. **b** and **c** are two additional examples of the fracture surfaces. Insets in **b** and **c** show the overview of the broken NWs attached on the cantilevers.